Targeting the cuproptosis-associated gene COL22A1 in glioblastoma using EMD-1204831 and kaempferol

YI CHEN[1,2*], YE ZHANG[2*], HUILAN YANG[3*], QIANG LIU[2], RUI SUI[2], JI SHI[2], HAIYANG LIANG[2], JIA LIU[2], HUIZHE XU[4] and HAOZHE PIAO[2,4]

[1]Graduate School, Dalian Medical University, Dalian, Liaoning 116044, P.R. China; [2]Department of Neurosurgery, Cancer Hospital of China Medical University, Cancer Hospital of Dalian University of Technology, Liaoning Cancer Hospital and Institute, Shenyang, Liaoning 110042, P.R. China; [3]Department of Hyperbaric Oxygen, The Second Affiliated Hospital of Shenyang Medical College, Shenyang, Liaoning 110003, P.R. China; [4]Central Laboratory, Cancer Hospital of China Medical University, Cancer Hospital of Dalian University of Technology, Liaoning Cancer Hospital and Institute, Shenyang, Liaoning 110042, P.R. China

Received May 31, 2024; Accepted December 11, 2024

DOI: 10.3892/ijo.2025.5744

Abstract. Glioblastoma (GBM) is a disease with high morbidity and poor prognosis. The combination of traditional Chinese and Western medicine and cuproptosis are known to serve important roles in the treatment of GBM. However, targeting cuproptosis to treat GBM by combining traditional Chinese and Western medicine has not been extensively investigated. Therefore, the present study focused on the diagnosis and treatment of GBM based on cuproptosis. Through a bioinformatics approach, a cuproptosis-related prognostic model was first constructed. Next, this prognostic model was found to be closely related to immune infiltration, DNA mutation and DNA methylation through multi-omics analysis. The present study indicated the cell clusters in GBM tissues and the risk scores in each cluster based on single-cell sequencing data derived from Gene Expression Omnibus. Notably, by screening the CellMiner database, EMD-1204831 was found to exhibit a high correlation with the risk score. Next, through network pharmacology and molecular docking analysis, the risk score-related gene collagen type XXII α1 chain (COL22A1) was identified as the target of kaempferol, which is the active component of Ginseng. Notably, kaempferol could decrease the proliferation of GBM cells by inhibiting COL22A1 expression in cell experiments. Finally, kaempferol and EMD-1204831 had an obvious inhibitory effect on the growth of GBM and sensitized GBM to cuproptosis inducers via COL22A1 in cell and animal experiments. Overall, the present study revealed a cuproptosis-related combined regimen for GBM.

Introduction

Glioma is the most common malignant tumor of the nervous system, with high malignancy, fast growth, a short disease course, ease of recurrence and a high incidence of postoperative complications (1,2). Glioma is considered to be one of the most challenging and drug-resistant tumors in neurosurgical treatment (3). Thus, it is urgent to identify novel treatments for glioblastoma (GBM).

Copper is an integrant mineral for life and an important component of numerous vital activities, including biological oxidation-reduction, iron metabolism, antioxidant effects and detoxification (4). Copper has also been reported to promote angiogenesis, which is important for tumor progression and metastasis. Researchers have identified a novel method of cell death, cuproptosis, that differs from known cell death types. Direct copper binding to the fatty acylation component of the tricarboxylic acid cycle results in cuproptosis, causing aggregation of fatty acylated proteins and iron loss (5). The synthesis of sulfur cluster proteins results in proteotoxic stress, in turn causing cell death (5). The potential impact of copper on the development of cancer cells has been the subject of numerous investigations (5,6). Copper has a strong affinity for MEK1 and binds to it directly. By activating ERK1/2 downstream, it stimulates the growth of tumors (6). Disruption of copper homeostasis reportedly triggers cuproptosis, thereby synergizing with regorafenib-mediated lethal inhibition of autophagy in GBM. Therefore, Cu^{2+} and regorafenib may serve a role in the treatment of GBM by regulating autophagy and

Correspondence to: Dr Huizhe Xu, Central Laboratory, Cancer Hospital of China Medical University, Cancer Hospital of Dalian University of Technology, Liaoning Cancer Hospital and Institute, 44 Xiaoheyan Road, Dadong, Shenyang, Liaoning 110042, P.R. China
E-mail: xuhuizhe@cancerhosp-ln-cmu.com

Professor Haozhe Piao, Department of Neurosurgery, Cancer Hospital of China Medical University, Cancer Hospital of Dalian University of Technology, Liaoning Cancer Hospital and Institute, 44 Xiaoheyan Road, Dadong, Shenyang, Liaoning 110042, P.R. China
E-mail: piaohaozhe@cancerhosp-ln-cmu.com

*Contributed equally

Abbreviations: GBM, glioblastoma; FDX1, ferredoxin 1; ROS, reactive oxygen species; GSEA, gene set enrichment analysis; TCGA, The Cancer Genome Atlas; AUC, area under the curve

Key words: GBM, cuproptosis, immune cell infiltration, single-cell RNA sequencing, collagen type XXII α1 chai

cuproptosis (7). Ferredoxin 1 (FDX1), a pivotal determiner of cuproptosis, works by using ferredoxin reductase to transport electrons from NADPH to cytochrome P450 (8). Unlike the majority of malignancies, GBM multiforme, gastric adenocarcinoma and endometrial cancer all exhibit high levels of FDX1 expression (9). High FDX1 expression is inversely related to the prognosis of patients with GBM (9). Research has reported the possibility of reducing copper levels in patients with newly diagnosed GBM. The safety profile is consistent with the known toxicity profile, and primarily related to hematology, penicillamine and copper deficiency (10). A phase II trial of penicillamine for copper depletion and anti-angiogenic therapy in GBM is underway (10). Copper has also been found to induce GBM cell senescence by downregulating B lymphoma Mo-MLV insertion region 1 homolog. Therefore, by inducing premature senescence in GBM cells, it may provide a useful *in vitro* model for the development of novel tumor therapeutic strategies (11). Disulfiram combined with copper can improve the efficacy of temozolomide in the treatment of GBM (12). Cuproptosis-related genes have also been used in tumor diagnosis. Solute carrier family 31 member 1 has been selected as a potential cuproptosis-related gene in breast cancer because its expression was upregulated, and exhibited the ability to predict diagnosis, prognosis and drug response (13). Cuproptosis-related signatures help predict prognosis and guide treatment in patients with hepatocellular carcinoma (14). Cuproptosis serves an important role in tumors, and the levels of cuproptosis, prognosis, diagnosis and mechanisms of immune responses in different tumors warrant further study.

EMD-1204831 was first developed and synthesized by Merck Serono; Merck KGaA. It could highly selectively inhibit c-Met receptor tyrosine kinase activity in both a ligand-dependent and -independent manner (15). In mice with ligand-dependent Hs746T and hepatocyte growth factor-dependent U87MG cancer, EMD-1204831 treatment was associated with potent tumor growth suppression and regression; however, to the best of our knowledge, the specific mechanism of action is unknown (15). Since studies of EMD-1204831 in GBM are not precise enough, a comprehensive mechanistic analysis of its anti-GBM action was conducted.

Materials and methods

Data collection. The Cancer Genome Atlas (TCGA; https://portal.gdc.cancer.gov/) and Chinese Glioma Genome Atlas (CGGA; https://www.cgga.org.cn/) were mined to collect data of patients with GBM and clinical information, which included tumor tissues and normal tissues from healthy controls (TCGA, TCGA-GBM; CGGA, mRNAseq_693). The transcript information of patients with GBM was obtained from the GSE100675 dataset in the Gene Expression Omnibus (GEO) database (https://www.ncbi.nlm.nih.gov/geo/), including 19 control individuals and 19 patients with GBM. The transcripts per kilobase of exon model per million mapped reads method was used for data normalization. The CGGA dataset was used for the consensus analysis. TCGA data were used to construct the least absolute shrinkage and selector operator (LASSO) model. The GSE100675 dataset was used to perform differentially expressed gene (DEG) analysis. The cuproptosis-related genes, including FDX1, LIPT1, DLD, LIAS, dihydrolipoamide S-acetyltransferase (DLAT), PDHA1, PDHB, MTF1, GLS and CDKN2A, were obtained from a previous study (5).

DEG analysis. The R (R-4.2.0; https://www.r-project.org/) package limma (3.58.1; https://www.bioconductor.org/packages/release/bioc/html/limma.html) was used for DEG analysis. Statistically, genes were considered significantly differentially expressed when log|fold change|≥1 and $P<0.05$. Additionally, for cuproptosis-related genes in TCGA-GBM dataset, consensus clustering was conducted using the ConsensusClusterPlus (1.70.0; https://bioconductor.org/packages/release/bioc/html/ConsensusClusterPlus.html) R package, and principal component analysis was performed to visualize the distribution of subtypes.

Gene set enrichment analysis (GSEA). After obtaining the DEGs, GSEA was performed to assess enrichment based on Gene Ontology terms and signaling pathways related to these genes. This process was performed using the enrichplot (1.22.0; https://bioconductor.org/packages/release/bioc/html/enrichplot.html) and clusterprofiler (4.10.0; https://www.bioconductor.org/packages/release/bioc/html/clusterProfiler.html) packages in R. Enrichment results were considered statistically significant when $P<0.05$.

LASSO regression analysis. A risk score model was constructed using LASSO regression. First, univariate Cox proportional hazard regression analysis was implemented by applying the R package survival (3.5-7; https://cran.r-project.org/web/packages/survival/index.html) and genes related to overall survival (OS) were identified. Next, to screen the most characteristic genes among them, LASSO regression analysis was performed, where the dataset from TCGA was selected as the training set and the dataset from CGGA was selected as the verification set. The risk score was calculated using the following formula: Risk score=$\sum$(Xi x Coefi), where Xi is the normalized expression value of the gene and Coefi is the coefficient.

Single-cell RNA sequencing (scRNA-seq) analysis. For scRNA-seq analysis, the Seurat package in R (5.0.2; https://cran.r-project.org/web/packages/Seurat/index.html) was used to analyze the GSM6432709 dataset from GEO (16). First, the data were preprocessed and all batch effects were removed. The data were clustered using the FindCluster function, and the marker genes of each cell cluster were obtained using the Findmarkers function. The Monocle3 package (4.1.0; https://cole-trapnell-lab.github.io/monocle3/docs/installation/) was also used to perform pseudotemporal trajectory analysis to explore the relationship between the prognostic genes and disease development.

Protein level validation of central genes. The Human Protein Atlas (https://www.proteinatlas.org/) is designed to create human proteome-wide maps. To validate the protein expression levels of the nine genes [AE binding protein 1 (AEBP1), NOP2/Sun RNA methyltransferase 5 (NSUN5), MED10,

CCM2 scaffold protein (CCM2), oncostatin M receptor (OSMR), ribosomal protein L39 like (RPL39L), EN2, collagen type XXII α1 chain (COL22A1) and DNAJC3] obtained from the LASSO regression analysis, the protein expression levels of target genes in the Human Protein Atlas were screened in patients with colon, breast and lung cancer.

Immune cell infiltration analysis. To analyze immune infiltration in GBM, the dataset was divided into high-risk and low-risk groups, and the control and disease groups from the dataset were compared. This analysis process was performed using the Cibersort (R script v1.04; https://cibersortx.stanford.edu/) algorithm. When P<0.05, the analysis results were considered statistically significant.

DNA methylation analysis. A dataset from TCGA was used in the present study. First, quality control and normalization analysis were performed on the dataset (Benjamini-Hochberg correction; P<0.05). Subsequently, differential methylation sites (Δβ values >0.1) were obtained using the ChAMP package in R (2.36.0; https://www.bioconductor.org/packages/release/bioc/html/ChAMP.html).

Somatic mutation analysis. The somatic mutation data of GBM samples were downloaded from TCGA. The mutation data were analyzed and visualized using the maftools package in R (2.22.0; https://www.bioconductor.org/packages/release/bioc/html/maftools.html).

Drug sensitivity analysis. The CellMiner tool (v2.9; https://discover.nci.nih.gov/cellminer/home.do) was used for drug susceptibility analysis. Drugs with high sensitivity [correlation coefficient (cor) >0.3; P<0.05] were screened. Next, the relationship between drugs and target genes was visualized through box plots and correlation curves.

Collection of active ingredients of Ginseng. The Traditional Chinese Medicine Systems Pharmacology database (TCMSP) was investigated to determine the ingredients of Ginseng (https://old.tcmsp-e.com/tcmsp.php). This database includes a set of ingredients, targeted genes and pharmacokinetic properties of natural compounds. To determine the active ingredients of Ginseng in the database, the screening criteria were: Oral bioavailability ≥30% and drug-likeness ≥0.18.

Molecular docking. Molecular docking tools were used to analyze the interaction between the predicted drugs and the target genes. This was performed using AutoDock software (v1.2.x; https://autodock.scripps.edu/), and the results were visualized using Discovery Studio Visualizer (v.19; https://discover.3ds.com/discovery-studio-visualizer-download) software.

Cell culture. The pharmacological experiments in the present study were conducted using GBM cells. The 293T, LN229 and A172 cells obtained from American Type Culture Collection were grown in DMEM (Gibco; Thermo Fisher Scientific, Inc.) supplemented with 10% fetal bovine serum (Gibco; Thermo Fisher Scientific, Inc.) and 1% penicillin and streptomycin (Gibco; Thermo Fisher Scientific, Inc.) at 37˚C in an incubator with 5% CO_2.

Transfection. To silence COL22A1, short hairpin RNA (shRNA/sh) specific to COL22A1 (shCOL22A1-1, 5'-GGTCTTGTTTAGAGTCTGA-3'; shCOL22A1-2, 5'-GTCTGAGTTTGTGAGATTA-3') and negative control shRNA (shNC; 5'-CAACAAGATGAAGAGCACCAA-3') were designed and synthesized by Sangon Biotech Co., Ltd. The 2nd generation system was used to generate lentivirus. The shRNA was integrated into the pLKO.1 vector (2 μg; 8453; Addgene, Inc.), and transfected into 293T cells along with psPAX2 (1 μg; 8454; Addgene, Inc.) and PMD2.G (1 μg; 12260; Addgene, Inc.) using Lipofectamine® 2000 (Thermo Fisher Scientific, Inc.) for 48 h at 37˚. Viruses were collected at 48 and 72 h and filtered using a 0.45-μm nitrocellulose filter. Polyethylene glycol 6000 was added and the viruses were concentrated by ultracentrifugation (4˚C; 1,500 x g; 30 min). Subsequently, the virus was added to the cells for 2 days. Target cells were infected with virus using polybrene (8 mg/ml). The multiplicity of infection used to infect cells was 10. The next day, the cells were selected with puromycin for 48 h (2-5 μg/ml; MilliporeSigma). The transfection efficiencies were detected by western blotting. Next, the cells were used for subsequent experiments. The time interval between transduction and subsequent experimentation was ~5 days. Puromycin (1-2 μg/ml; MilliporeSigma) was used for maintenance.

Cell Counting Kit-8 (CCK-8) assay. To study cell proliferation following drug intervention, LN229 and A172 cells were treated with DMSO (<0.1% v/v; HY-Y0320; MedChemExpress), kaempferol (80 μM; HY-14590; MedChemExpress), EMD-1204831 (9 μM; HY-164394; MedChemExpress), the combination of kaempferol (9 μM) and EMD-1204831 (80 μM) or elesclomol (HY-12040; MedChemExpress) for 24 h at 37˚C, and CCK-8 cell viability experiments (Merck KGaA) were conducted. First, 5,000 cells per well were seeded in 96-well plates. Cells were collected and the CCK-8 reagent (10 μl per well) was added at 72 h for incubation for 2 h in the dark at 37˚C with 5% CO_2. The VersaMax microplate reader (Molecular Devices, LLC) was used to measure absorbance at a wavelength of 450 nm.

Cell colony formation assay. A cell colony formation experiment was conducted to assess cell proliferation. A total of $2x10^3$ LN229 and A172 cells were grown for 14 days on 6-well plates and treated with DMSO, kaempferol (80 μM), EmdMD-1204831 (9 μM) or the combination of both at 37˚C for 24 h. When there were >50 cells for a single cell clone, cloning was deemed complete. The cells were then dyed with viola crystallina for 30 min at 37˚C after fixation with 10% paraformaldehyde (Thermo Fisher Scientific, Inc.) for 30 min at room temperature. Subsequently, the clone numbers were counted manually. The definition of colonies was >50 cells for a single cell clone.

Transmission electron microscopy. For electron microscopy analysis, tumors were dissected (1 mm^3) in an ice-cold fixative (2.5% glutaraldehyde in 0.1 mol/l PIPES buffer at pH 7.4). After 10 h of fixation at 4˚C, samples were washed with 0.1 mol/l PIPES, post-fixed in 1% OsO_4 (30 min at room temperature) and stained in 2% uranyl acetate (1 h at room temperature). Samples were dehydrated in an ethanol series (50, 70 and

100%) and embedded in epoxy (37˚C; overnight; 12-16 h). The tissues were divided into ~70 nm slices. The slices were observed and images were captured with a HT-7700 transmission electron microscope.

Ki67 staining. Tumor tissues were stained using Ki67 antibody (9027; 1:400; Cell Signaling Technology, Inc.) and Ki67-positive cells were counted as described previously (17). The results of Ki67 staining were recorded as the percentage of Ki67-positive cells.

Mice. A total of 20 male BALB/c-nude mice (6 weeks; weight, 17-21 g) from Shanghai Model Organisms Center, Inc. were stochastically separated into four groups, with 5 mice in each group. The housing conditions were as follows: Temperature, 20-26˚C; humidity, 50-70%; light/dark cycle, 12 h/12 h; and feeding food and water in the cage every day. A total of $5x10^6$ LN229 cells were resuspended in 1 ml PBS, 8 μl ($4x10^4$) of which were stereotactically injected into the right hemisphere of the brain, at 0.5 mm posterior of the bregma, 2 mm to the right of the sagittal suture and 3 mm below the surface of the skull. Deep anesthesia was used to control and treat pain (isoflurane; induction, 4-5%; maintenance, 2%). The cells were injected into the brain through microsyringes. When the volume of the tumor reached 100 mm^3, the four groups of mice were treated as follows: No treatment in the control group, injection of EMD-1204831 (10 mg/kg), injection of kaempferol (20 mg/kg) and simultaneous injection of EMD-1204831 and kaempferol. The drugs were injected every 2 days. The tumor cells were infected with lentivirus generating luciferase and tumor growth was monitored by bioluminescent imaging. Tumor volumes were measured every 4 days. Tumors were peeled off for testing. Mice were euthanized by intraperitoneal injection of sodium pentobarbital (100-200 mg/kg) after 4 weeks. The tumors were examined by H&E staining according to the protocol in the kit (fixation with 4% paraformaldehyde for 6-8 h at room temperature; thickness of sections, 5 μm; staining with haematoxylin for 4 min, hydrochloric acid alcohol for 3 sec and eosin for 25 sec-1 min; all staining steps were performed at room temperature; type of microscope used, light microscope). After euthanasia, the death of the animals was confirmed based on the disappearance of pain response, no response when pressing the toes with hands or forceps, and observation of cardiac and respiratory arrest. The time interval between injection/implantation and the final tumor growth measurement was ~28 days.

Reactive oxygen species (ROS) assay. A ROS detection kit (C10445; Invitrogen; Thermo Fisher Scientific, Inc.) was used to detect the levels of ROS in LN229 and A172 glioma cell lines treated with $CuCl_2$ and the cuproptosis inducer elesclomol (STA-4783; MedChemExpress). Firstly, GBM carcinoma cells in the logarithmic growth phase were inoculated into a 12-well plate and further cultured. When the cell density reached 40-50%, 200 nM elesclomol was added to treat the cells for 24 h at 37˚C, followed by the addition of 10 μM ROS fluorescence probe (S0033S; Beyotime Institute of Biotechnology) for incubation at 37˚C for 20 min. Finally, flow cytometry (BD LSRFortessa; BD Biosciences) was used to detect the intensity of the fluorescence signals at an excitation wavelength of 488 nm, which represented the levels of ROS (fluorescence emission: Before lipid peroxidation, analyte detector, 581 nm, analyte reporter, 591 nm; after lipid peroxidation, analyte detector, 488 nm, analyte reporter, 510 nm). Lipid peroxidation was determined by quantitating the fluorescence intensities and calculating the ratio of intensity in the Texas Red® channel (581/591 nm) to the intensity in the FITC channel (488/519 nm). Flowjo v9 software (BD Biosciences) was used.

Measurement of intracellular copper. A total of $2x10^5$ LN229 and A172 GBM cells per well in the logarithmic growth phase were inoculated into a 6-well plate and cultured for 12 h. Subsequently, cells were incubated with different concentrations of $CuCl_2$ (0, 0.5, 1, 2, 2.5, 3, 4 and 5 μmol/l) to generate a standard curve (data not shown) and the cuproptosis inducer elesclomol (200 nM) for 24 h at 37˚C. Cells were collected and resuspended in 120 μl water. Ultrasound was used to break the cells to collect copper ions inside the cells. Finally, copper ions inside the cells were detected according to the instructions (E-BC-K775-M; Elabscience Bionovation Inc.) using a microplate reader.

Western blotting. LN229 and A172 glioma cells in the logarithmic growth phase were inoculated into a 6-well plate, and the cells were cultured until they reached a density of 40-50%. Different concentrations of $CuCl_2$ (0, 0.5, 1, 2, 2.5, 3, 4 and 5 μmol/l) and the cuproptosis inducer elesclomol (200 nM) were added to treat the cells at 37˚C overnight. The cells were washed with PBS once. Total protein was extracted from the cells with an appropriate amount of RIPA lysis buffer (P0013C; Beyotime Institute of Biotechnology) and the protein concentration was measured using a BCA kit (23225; Thermo Fisher Scientific, Inc.). The mass of protein loaded per lane was ~100 μg. The percentage of the SDS-PAGE gel was 10%. The expression of proteins was detected through western blotting. Proteins were transferred to nitrocellulose membranes. The membranes were blocked in 5% milk containing 2% BSA (A8020; Beijing Solarbio Science & Technology Co., Ltd.) at room temperature for 1 h. Membranes were incubated at 4˚C overnight (12-16 h) with the primary antibodies, including COL22A1 (1:2,000; PA5-70816; Invitrogen; Thermo Fisher Scientific, Inc.), DLAT (1:3,000; cat. no. 13426-1-AP; Proteintech Group, Inc.), dihydrolipoamide S-succinyltransferase (1:10,000; cat. no. ab177934; Abcam), FDX1 (1:2,000; cat. no. 12592-1-AP; Proteintech Group, Inc.), ACTB (1:3,000; ab8226; Abcam) and GAPDH (1:50,000; cat. no. 60004-1-Ig; Proteintech Group, Inc.) antibodies, then washed with PBS with 0.5% Tween-20 three times, and an appropriate amount of the HRP-conjugated secondary antibody was added for incubation at room temperature for 1 h (anti-mouse IgG; 1:5,000; ab7068; Abcam; anti-rabbit IgG; 1:5,000; ab288151; Abcam). An ECL kit was used for visualization (322209; Thermo Fisher Scientific, Inc.). Images were captured using the BIO-RAD ChemiDoc MP multifunctional chemical imaging instrument (Bio-Rad Laboratories, Inc.).

Statistical analysis. Kaplan-Meier plots were plotted and the log-rank test was performed to estimate and compare the OS

between the two risk groups in the training set. The Renyi test was performed to estimate and compare the OS between the two risk groups in the verification set. The hazard ratio and Cox P-values were generated using Cox analysis. The correlations between different factors were analyzed using Spearman's statistical methods. Statistical analysis was performed using GraphPad Prism 8.0 software (Dotmatics). Data are presented as the mean ± standard deviation of three experimental repeats. An unpaired Student's t-test was used for comparisons between two groups. Differences among multiple groups were analyzed by one-way ANOVA followed by Tukey's post hoc test. Differences among multiple groups containing two variables were analyzed using two-way ANOVA followed by Bonferroni's post hoc analysis. The tumor volumes of mice in different drug groups were analyzed using two-way mixed ANOVA with the Bonferroni post hoc test. The immune cell infiltration based on Cibersort was analyzed using the Wilcox rank-sum test. $P<0.05$ was considered to indicate a statistically significant difference.

Results

Consensus clustering of cuproptosis-related genes in patients with GBM. Although cuproptosis has been shown to serve an important role in GBM (9), to the best of our knowledge, the precise mechanism of its action remains unknown. First, the present study grouped the GBM cohort (k=3) by consensus clustering analysis according to cuproptosis-related genes, which means there were three cuproptosis levels (high, middle and low; Figs. 1A, and S1A and B). Next, different cuproptosis levels of patients will be associated with different outcomes. For example, high cuproptosis levels of patients are associated with a longer OS than low cuproptosis levels (18). Therefore, to identify the high and low groups of cuproptosis levels in patients, survival analysis for the three groups was performed and the results revealed that the prognosis of cluster 2 and 3 was significantly better than that of cluster 1, and cluster 2 had a longer OS than cluster 3, thus cluster 2 was considered as relative high level of cuproptosis and cluster 3 as cuproptosis low level because the OS in cluster 2 was longer than that in cluster 3 (18) (data not shown). Therefore, groups 2 and 3 were selected for comparison. The survival performance of the former was improved according to the Kaplan-Meier analysis (P=0.00013; Fig. 1B). Subsequently, DEGs were compared between the two groups. As shown in Figs. 1C and D, and S1C, a total of 6,935 DEGs were identified, including 1,885 upregulated genes and 5,050 downregulated genes. GSEA verified that the DEGs were primarily gathered in 'cell cycle' pathways (Figs. 1E and F, and S1D). These results suggested that the cuproptosis-related DEGs were associated with malignant progression of GBM.

LASSO regression analysis for patients with GBM. To ascertain the characteristic genes associated with GBM prognosis, univariate Cox and LASSO regression analyses were conducted for an in-depth analysis of the identified DEGs. The candidate genes were screened by univariate Cox analysis (Fig. 2A). To eliminate analysis errors, the dataset from TCGA was used as the training set and characteristic prognostic genes were screened by LASSO analysis. As shown in Fig. 2B-D, nine prognostic genes were screened out. The risk score was calculated as follows: Risk score=AEBP1 x 0.007204771 + NSUN5 x 0.200917630 + MED10 x 0.257867168 + CCM2 x 0.017182529 + OSMR x 0.153430963 + RPL39L x 0.019123077 + EN2 x 0.038036644 + COL22A1 x 0.048587190 + DNAJC30 x 0.001146385. Based on the riskscore values in the patients with GBM from CGGA, the median value was calculated and the patients were divided into high and low risk groups according to the median value (Fig. S2A-C). Furthermore, the low-risk group exhibited improved survival performance compared with the high-risk group (Fig. 2E), and the 1-year area under the curve (AUC) value was 0.597 (Fig. 2F). The aforementioned results were confirmed in the validation set (Fig. 2G-K). The aforementioned findings showed that the prognostic model in the present study was closely associated with the prognosis of GBM and could predict the risk score of GBM based on the assessment of the risk score gene value of each patient.

Expression profiles of risk score-related genes. The DNA, mRNA and protein levels of these nine genes were assessed to examine the risk score-related genes in GBM. The DNA of *COL22A1*, *OSMR*, *NSUN5*, *AEBP1*, *CCM2* and *EN2* was mutated in GBM (Fig. 3A). Additionally, post-translational modification of DNA serves an important role in tumor regulation, and DNA methylation is one of the most common modification methods (19). Thus, the differentially expressed methylated genes were compared between the GBM group and the paracancerous group, and the methylation levels of numerous genes were significantly different between the two groups (Fig. 3B and D), which caused changes in their RNA levels (Figs. 3C and S3A). Next, the Human Protein Atlas database was queried and the protein expression levels of AEBP1, NSUN5, CCM2, OSMR, RPL39L and COL22A1 were found to be increased to varying degrees in tumor tissues of the colon (Fig. 3E). The result was validated in other cancer tissues (Fig. S3B). These results indicated that the status of most risk score-related genes was different at the multiomics level in GBM and normal tissues.

Somatic mutation analysis in GBM. Tumor occurrence is highly associated with DNA mutation (9). Mutation analysis was performed to examine DNA mutations in GBM. As shown in Fig. S4A, in the GBM group, the mutation frequencies of PTEN, TP53, EGFR and TTN were the highest. The mutation frequencies of the high-risk group and low-risk group were different (Fig. S4B and C). Therefore, the prognostic model in the present study was closely related to DNA mutation.

Biofunction analysis of risk score-related genes via scRNA-seq. Subsequently, to visualize the expression of risk score-related genes more accurately in different types of cells in GBM tissues, scRNA-seq was performed to analyze these genes. First, three cell populations that made up the GBM tissue were identified (Fig. 4A). Subsequently, risk scores of these cell populations were evaluated and risk score-related genes were highly expressed in malignant cells, which means that these risk score genes may exert their function mainly by

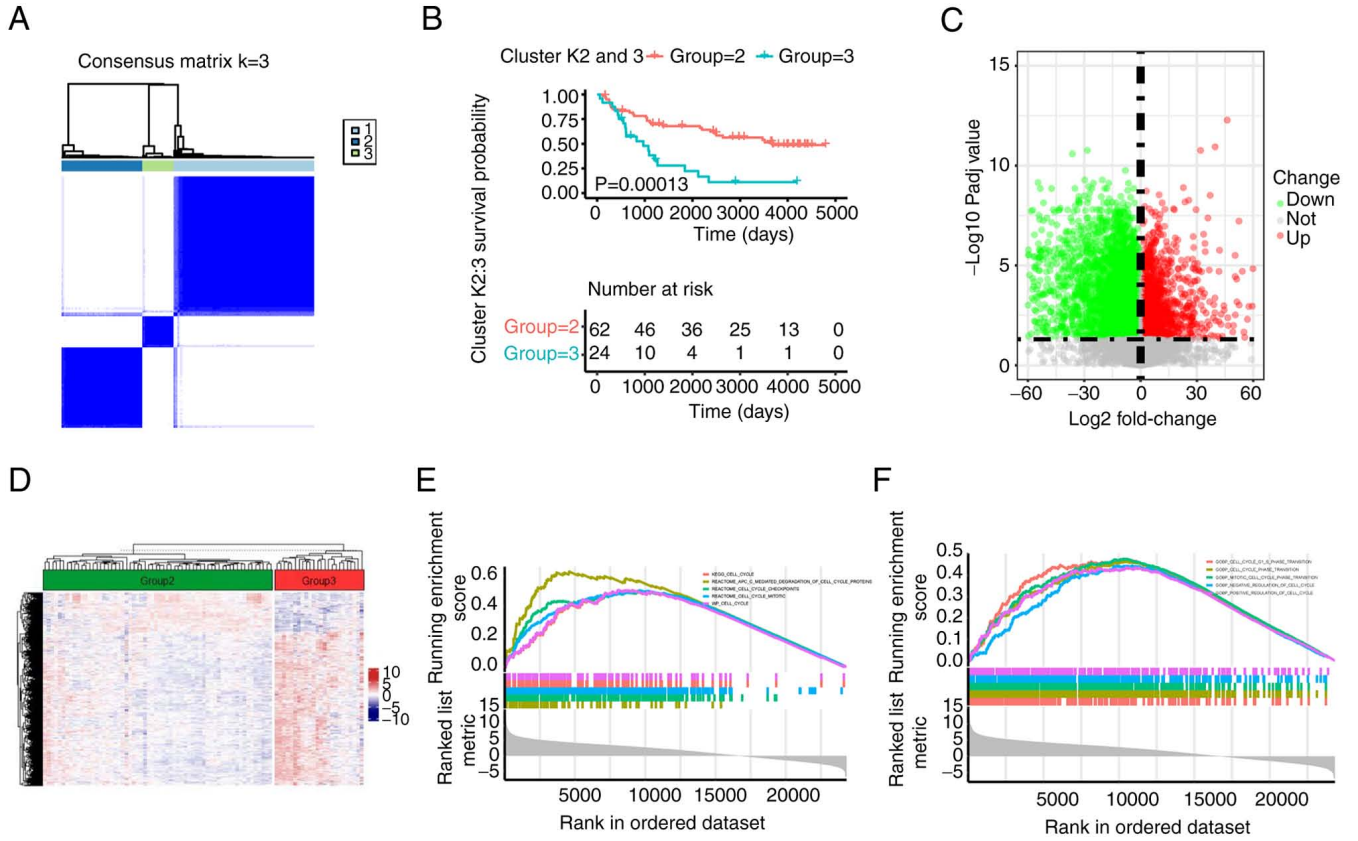

Figure 1. Consensus clustering of cuproptosis-related genes in patients with glioblastoma. (A) Consensus matrix of the Chinese Glioma Genome Atlas dataset with k=3. K2 and 3 means cluster group 2 and 3. Matrix means the data of CGGA. (B) Kaplan-Meier curves of progression-free survival probability of groups 2 and 3. Cuproptosis-related differentially expressed genes between groups 2 and 3 were visualized using a (C) volcano plot and (D) heatmap. The color indicates the expression levels of genes. Red indicates high expression levels and blue indicates low expression levels. (E) Top 5 cuproptosis-related gene sets enriched based on pathway GSEA. (F) Top 5 cuproptosis-related gene sets enriched based on GO GSEA. BP, biological process; GO, Gene Ontology; GSEA, gene set enrichment analysis; KEGG, Kyoto Encyclopedia of Genes and Genomes; Padj value, adjusted P-value.

influencing tumor cells (Fig. 4B and C). To further examine the dynamic changes in these genes during tumor development, a pseudo-timeline analysis was performed. As shown in Fig. 4D-F, the expression of these genes increased with tumor development. Simultaneously, the biomarkers based on a previous study (16) in each cell type were displayed using a heatmap (Fig. S5). The aforementioned findings of the scRNA-seq analysis further demonstrated the reliability of the prognostic model.

Immune cell infiltration analysis. Understanding the tumor-related immune microenvironment is crucial for understanding the occurrence and development of malignancies, since immune infiltration serves an important role in their formation (13). The present study used the Cibersort algorithm to examine the immune microenvironment in the high-risk group, low-risk group, GBM tumor group and paracancerous group. First, the proportions of different immune cell types in each group were examined. The proportion of different immune cell types in each group was analyzed, and there were significant differences in the degree of immune invasion of some B cells, macrophages and T cells not only in glioma and normal cells, but also in the high-risk group and the low-risk group (Figs. 5A-D and S6A-F). Based on the aforementioned results, it was concluded that the immune microenvironment changed during the development of GBM, and this change was closely related to the risk score.

Exploration of compounds and sensitive drugs targeting risk score-related genes. Integrative traditional Chinese and Western medicine is a current research hotspot in tumor treatment (20-22). First, traditional Chinese medicine (TCM) compounds targeting GBM were explored (Fig. 6A). Querying the TCMSP database showed that the Ginseng drug could only target the COL22A1 gene in the prognostic model (the other genes in the model could not be targeted by Ginseng), and the active ingredient was kaempferol (Fig. 6B). Fig. 6C shows the simulated binding sites. Further molecular docking analysis helped calculate the combining ability of the active ingredient and the targeted gene. The results were as follows: Kaempferol and COL22A1 score, -6.5 kcal/mol (Fig. 6D). To explore the therapeutic implications of the prognostic model, the risk score-related genes were subjected to a CellMiner drug sensitivity examination. The outcomes demonstrated that 386 medications were related to the prediction model risk score ($P<0.05$; $|cor|>0.3$). The drug tamoxifen exhibited a significant correlation and effect, while other drugs had no significant effect (Figs. 6E and F, and S7A and B). The results indicated that the COL22A1 gene in the prognostic model could be targeted by several drugs, suggesting that it possessed potential therapeutic significance.

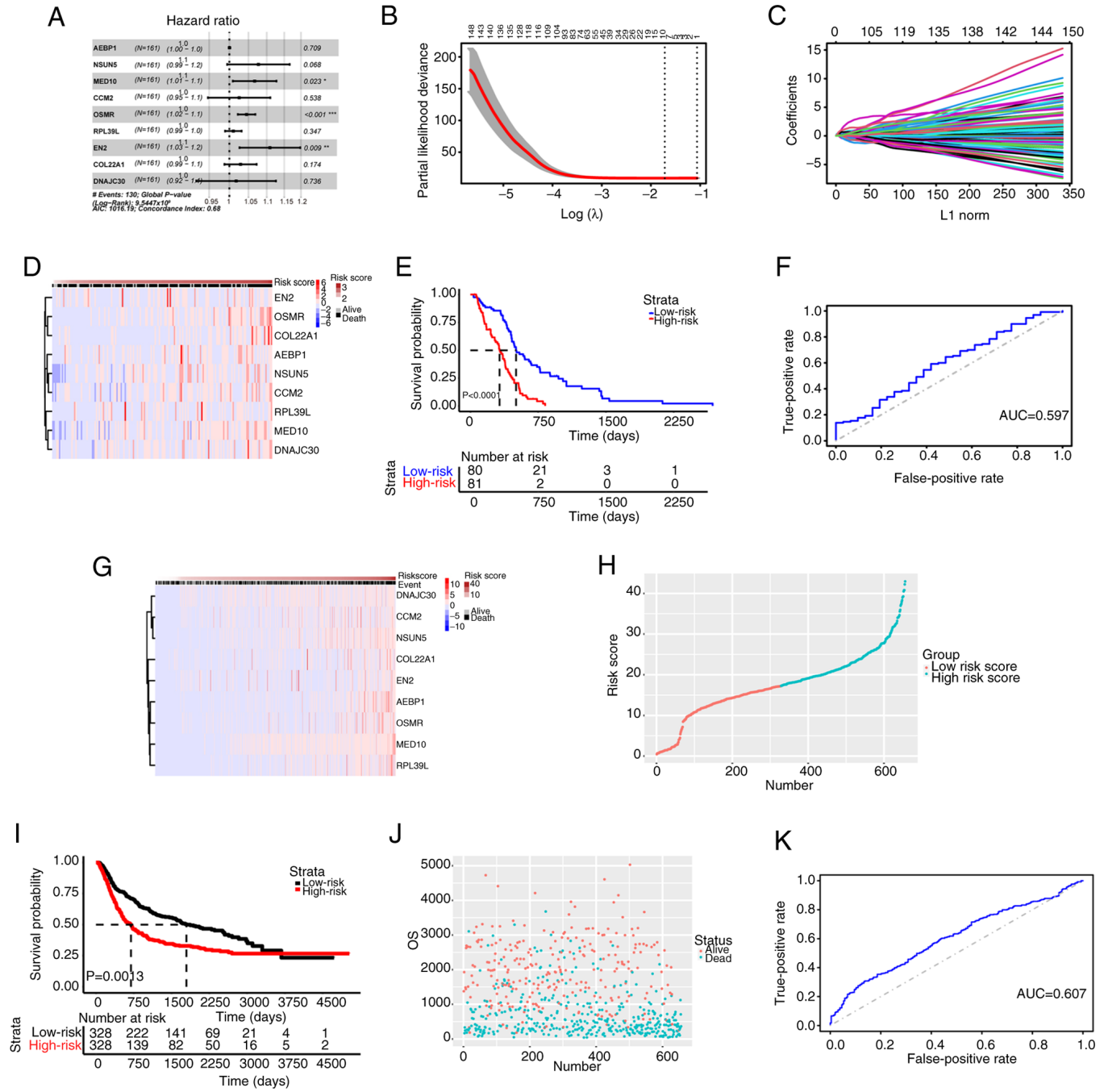

Figure 2. LASSO regression analysis for patients with glioblastoma. (A) Forest plot of risk score-related genes in the training set. (B) LASSO deviance profile of the 150 candidate genes. (C) LASSO regression coefficient profile of the 150 candidate genes. (D) mRNA expression profiles of nine risk score-related genes in a heatmap. (E) Survival probabilities of high-risk and low-risk groups. (F) ROC curve of the risk score of the training set. (G) mRNA expression of the nine risk score-related genes in the validation set. (H) Distribution of risk score in the low- and high-risk groups in the validation set. (I) Survival probabilities of the high- and low-risk score groups in the validation set. (J) Survival status of patients in the validation set. (K) ROC of the risk score of patients in the validation set. *P<0.05; **P<0.01; ***P<0.001. AIC, Akaike's Information Criterion; AUC, area under the curve; LASSO, least absolute shrinkage and selector operator; OS, overall survival; ROC, receiver operating characteristic.

Silencing COL22A1 enhances GBM cuproptosis. To verify the role of COL22A1 in the development of GBM, proliferation was detected using CCK-8 and colony formation assays, and the results demonstrated that inhibiting COL22A1 significantly decreased the proliferation and colony formation of GBM (Figs. 7A and B, and S8C and D). To further investigate the effect of COL22A1 on GBM cuproptosis, ROS levels were detected by flow cytometry. Low concentrations of elesclomol reduced ROS levels in the COL22A1 knockdown group, while this was not observed in the shNC group (Figs. 7C, and S8E and F). Copper concentrations were measured in the same groups, and the results were consistent with the aforementioned results; low concentrations of elesclomol significantly increased copper concentrations in the COL22A1 knockdown group, while this was not observed in the shNC group (Fig. 7D). Furthermore, the protein levels of the representative marker (FDX1) of cuproptosis were detected after knocking

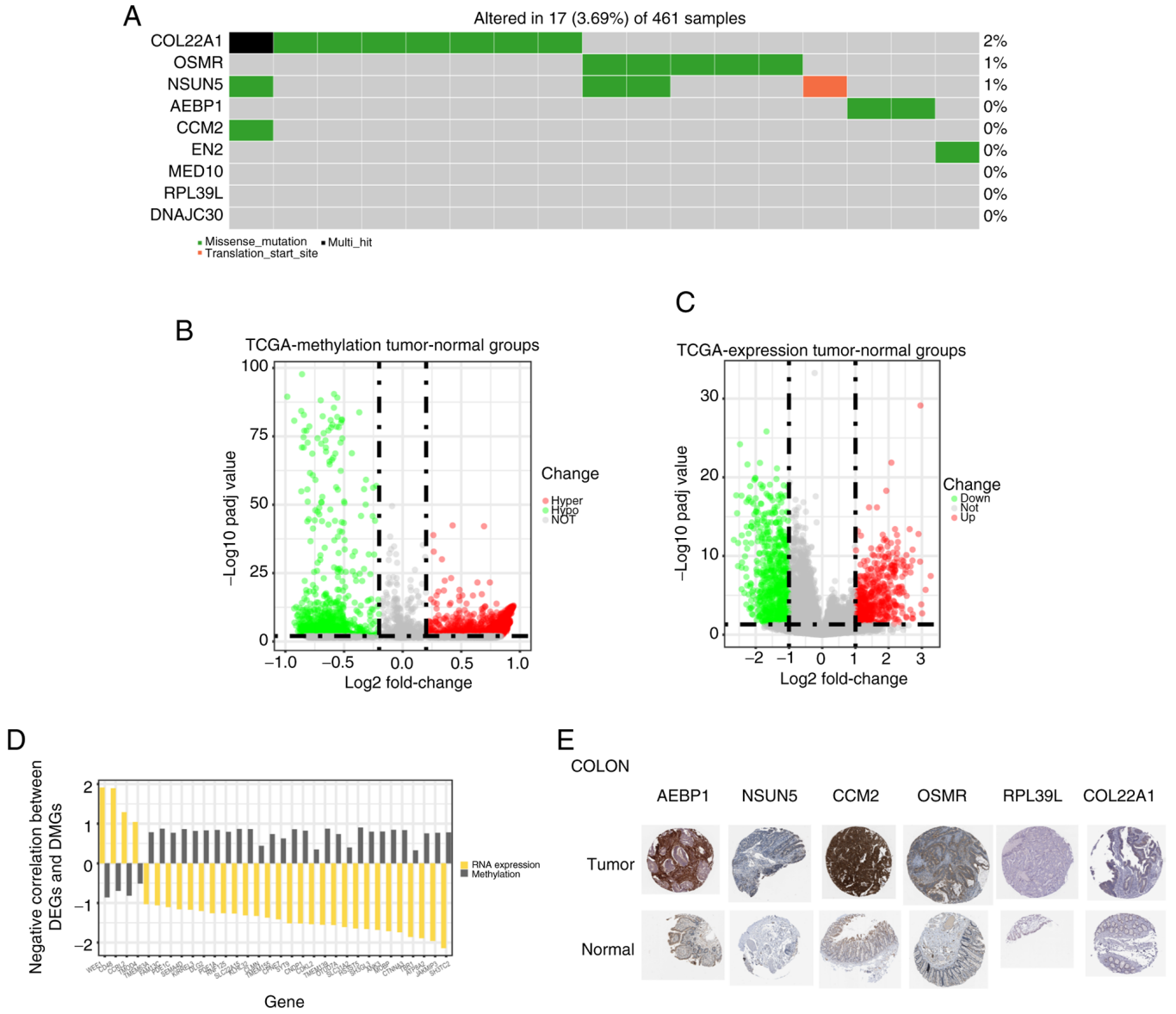

Figure 3. Expression profiles of risk score-related genes. (A) Somatic mutation of nine risk score-related genes in the dataset from TCGA. (B) Volcano plot of differential methylation sites in the tumor and normal groups. (C) Volcano plot of DEGs in the tumor and normal groups. (D) DEGs and DMGs with a negative correlation in the tumor and normal groups. (E) Representative immunohistochemistry images of six prognostic proteins in tumor and normal tissues of the colon. Magnification, x200. AEBP1, AE binding protein 1; CCM2, CCM2 scaffold protein; COL22A1, collagen type XXII α1 chain; DEG, differentially expressed gene; DMG, differentially methylated gene; NSUN5, NOP2/Sun RNA methyltransferase 5; OSMR, oncostatin M receptor; Padj value, adjusted P-value; RPL39L, ribosomal protein L39 like; TCGA, The Cancer Genome Atlas.

down COL22A1. The results showed that the levels of the downstream proteins of cuproptosis were decreased in shCOL22A1 cells treated with low concentrations of elesclomol compared with the shNC group (Fig. 7E). Similarly, transmission electron microscopy showed that low concentrations of elesclomol caused mitochondrial shrinkage in the shCOL22A1 group, which was not observed in shNC group (Fig. 7F). In conclusion, knockdown of COL22A1 promoted cuproptosis in GBM. Notably, EMD-1204831 and kaempferol inhibited COL22A1 expression, and the effect was greater when used in combination (Fig. 7G). Therefore, future studies should focus on the effect of the combination of EMD-1204831 and kaempferol on GBM development and cuproptosis.

EMD-1204831 and kaempferol synergistically treat GBM. The median effect concentration values of the two drugs were obtained through CCK-8 experiments in LN229 cells (Figs. 8A, and S8A and B). Subsequently, EMD-1204831 and kaempferol were used for treatment intervention in LN229 and A172 cells. The cell viability assay showed that the combined drugs reduced the cell activity more effectively than either drug alone, and their best concentrations of combination were determined (kaempferol, 80 μM; EMD-1204831, 9 μM) (Fig. 8B-D). Furthermore, the same results were obtained in colony formation assays (Fig. 8E). In order to further explore the combination effect of EMD-1204831 and kaempferol, LN229 cells were first injected into nude mice to prepare xenograft tumor models. The nude mice were divided into

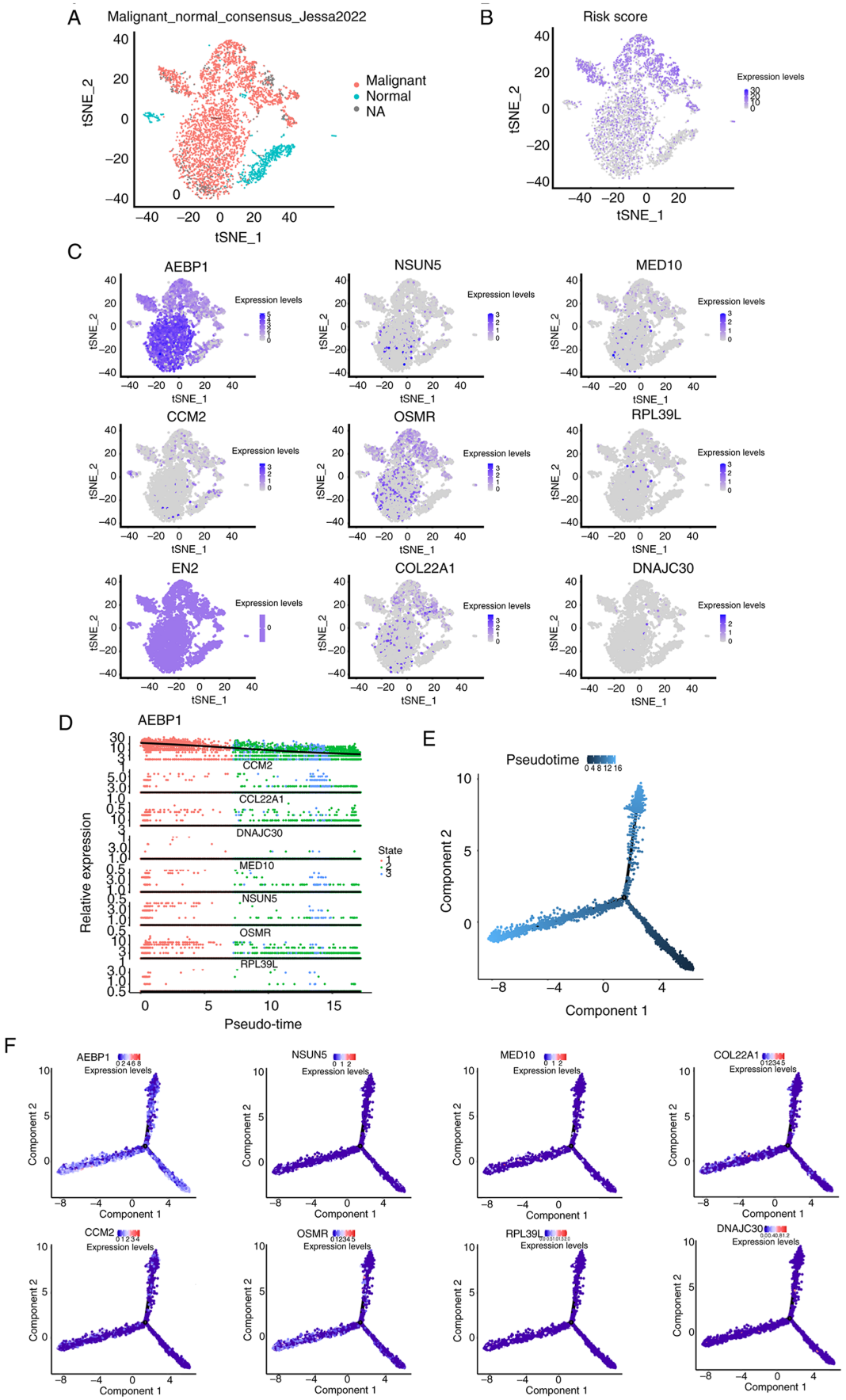

Figure 4. Biofunction analysis of risk score-related genes via single-cell RNA sequencing. (A) GBM tissues were categorized into three clusters (16). (B) Scatter plots of the risk score distribution. (C) Relative expression value of nine risk score-related genes in GBM cell states. (D) Trajectory of eight risk score-related genes. 1-3 represents the development period of tumors, which was divided into three stages, from 1 to 3. (E) Pseudotime trajectories of macrophages containing three main branches. (F) Pseudotime trajectories of macrophages containing three main branches for different genes. GBM, glioblastoma; NA, not applicable; tSNE, t-distributed stochastic neighbor embedding.

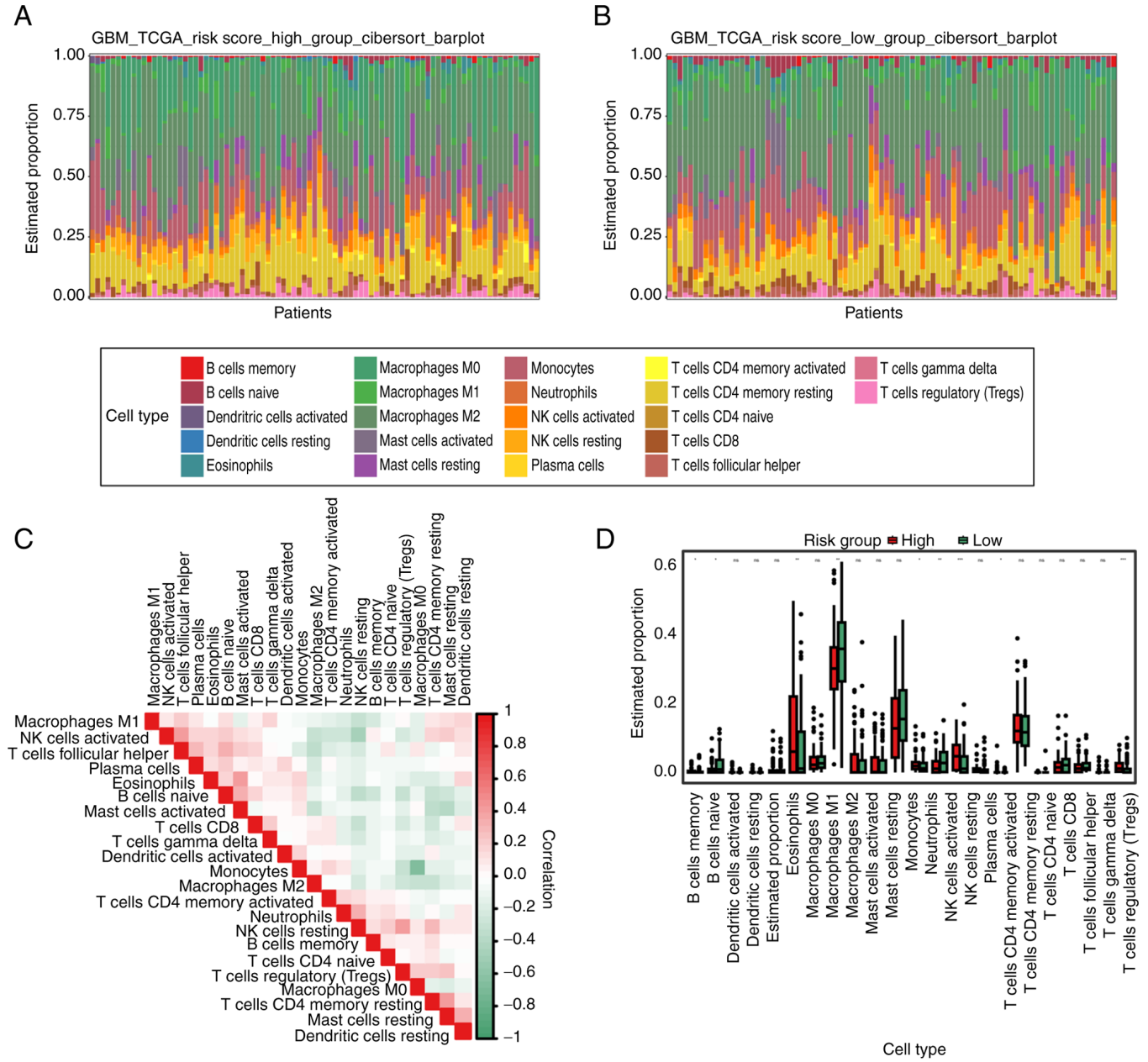

Figure 5. Immune cell infiltration analysis. (A) Mean proportion of 22 immune cell types in patients in the high-risk group. (B) Mean proportion of 22 immune cell types in the patients in the low-risk group. (C) Correlation matrix of all 22 immune cell proportions. (D) Differences in the 22 immune cell types between the high- and low-risk groups. *P<0.05; **P<0.01; ***P<0.001. GBM, glioblastoma; NK, natural killer; ns, not significant; TCGA, The Cancer Genome Atlas; Treg, regulatory T cell.

four groups, namely the vehicle, EMD-1204831, kaempferol and combination treatment groups. Compared with the vehicle group, the tumor volume and mass of the two groups of mice treated with either kaempferol or EMD-1204831 alone were reduced, while the tumor inhibition effect of the combined treatment group was the most obvious (Fig. 9A-C). After 4 weeks of treatment, tumor tissues were collected and Ki67 was examined. The proportion of positive tumor cells in the single drug groups was lower than that in the vehicle group, while the inhibitory effect in the combined drug group was greater (Fig. 9D). The results of the intracranial tumorigenesis experiment in mice were consistent with the results of the present *in vitro* experiments; the tumor size was smaller in the combined drug group than in the control and single drug groups (Fig. 9E and F). The aforementioned results indicated that the combination of EMD-1204831 and kaempferol had therapeutic effects on GBM both *in vivo* and *in vitro*.

Combination of EMD-1204831 and kaempferol sensitizes GBM to cuproptosis inducers. To clarify the effect of the combination of the two drugs on cuproptosis, the IC_{50} of the cuproptosis-inducer elesclomol was determined in GBM cell lines using a CCK-8 assay (Fig. 10A). Then, low concentrations of elesclomol (10 and 20 nM) were added in the control group and the combination group. The results of flow cytometry showed that the changes in ROS levels were not significant in the control group induced by low concentrations of elesclomol. Conversely, low concentrations of

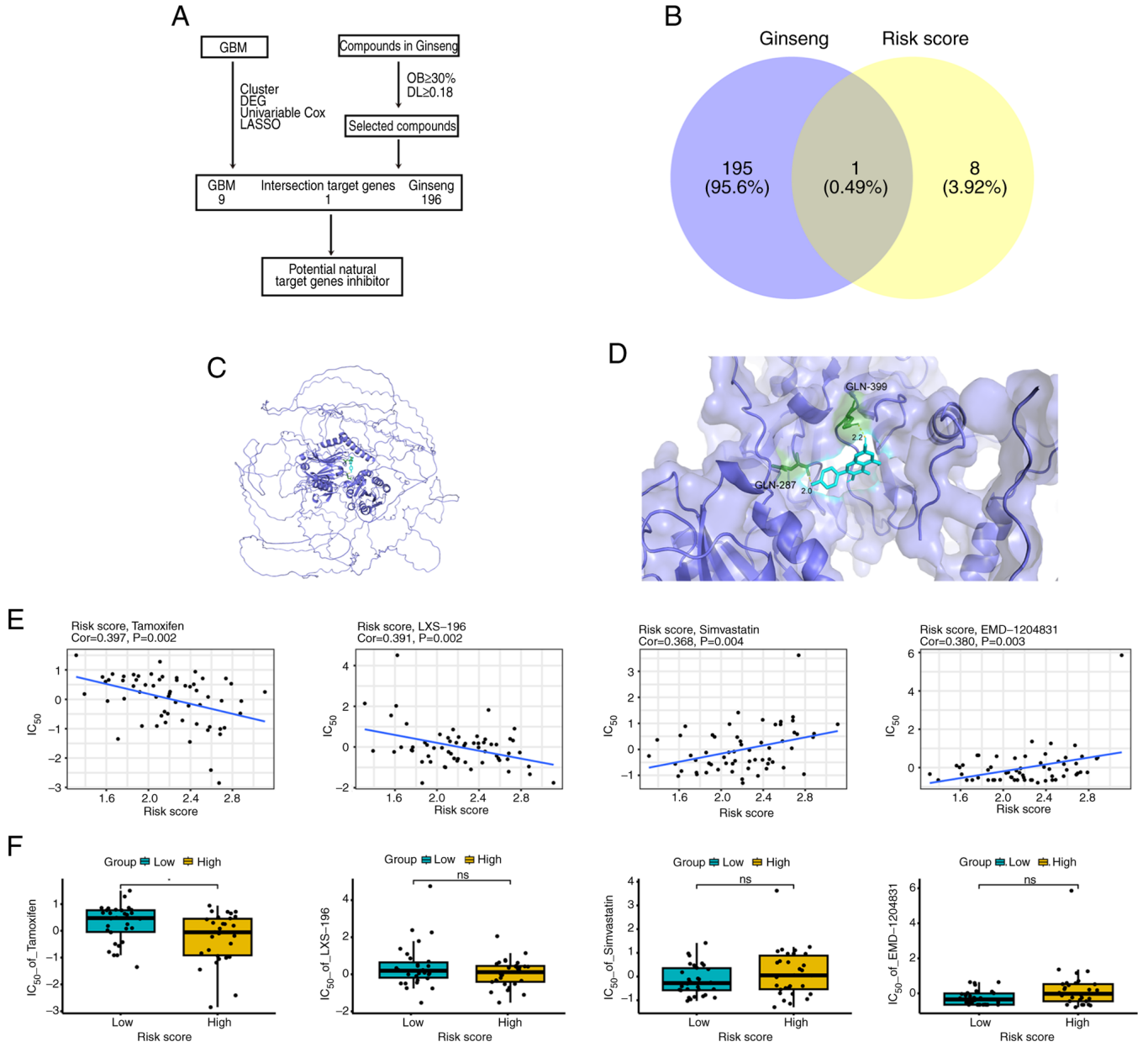

Figure 6. Exploration of compounds and sensitive drugs targeting risk score-related genes. (A) Overview of the molecular docking analysis procedure. (B) Venn diagram of Ginseng target genes and risk score-related genes. (C) 3D map of the binding of COL22A1 with kaempferol. (D) 3D map of the specific binding site of COL22A1 with kaempferol. (E) Correlation analysis and (F) box plot of drug sensitivity for different drugs in different risk score groups. COL22A1, collagen type XXII α1 chain; Cor, correlation coefficient; DEG, differentially expressed gene; DL, drug-likeness; GBM, glioblastoma; LASSO, least absolute shrinkage and selector operator; ns, not significant; OB, oral bioavailability.

elesclomol in the combination group (EMD-1204831 and kaempferol) significantly reduced ROS levels (Figs. 10B, and S8G and H). To further verify that the changes in ROS levels were related to cuproptosis, copper concentrations and cuproptosis checkpoint proteins were examined in both groups, and the results were consistent with the aforementioned results; compared with the DMSO group, the combination group exhibited increased copper concentrations and cuproptosis (the expression levels of FDX1 could reflect the levels of cuproptosis) (Fig. 10C and D). Furthermore, transmission electron microscopy showed that low concentrations of elesclomol caused mitochondrial shrinkage in the combination group, which was not observed in the DMSO group (Fig. 10E). In conclusion, the combination of EMD-1204831 and kaempferol increased the sensitivity of GBM to cuproptosis inducers.

Discussion

More than half of all gliomas are GBM, the most common primary malignant central nervous system tumor and the most aggressive, with the worst clinical prognosis (1). The standard treatment for GBM is based on surgery, combined with comprehensive treatments, including radiotherapy and chemotherapy; however, their efficacy is limited, with a median survival of 14-16 months (23,24). Cuproptosis is a recently reported novel form of death caused by excessive copper levels; however, the specific molecular mechanism of

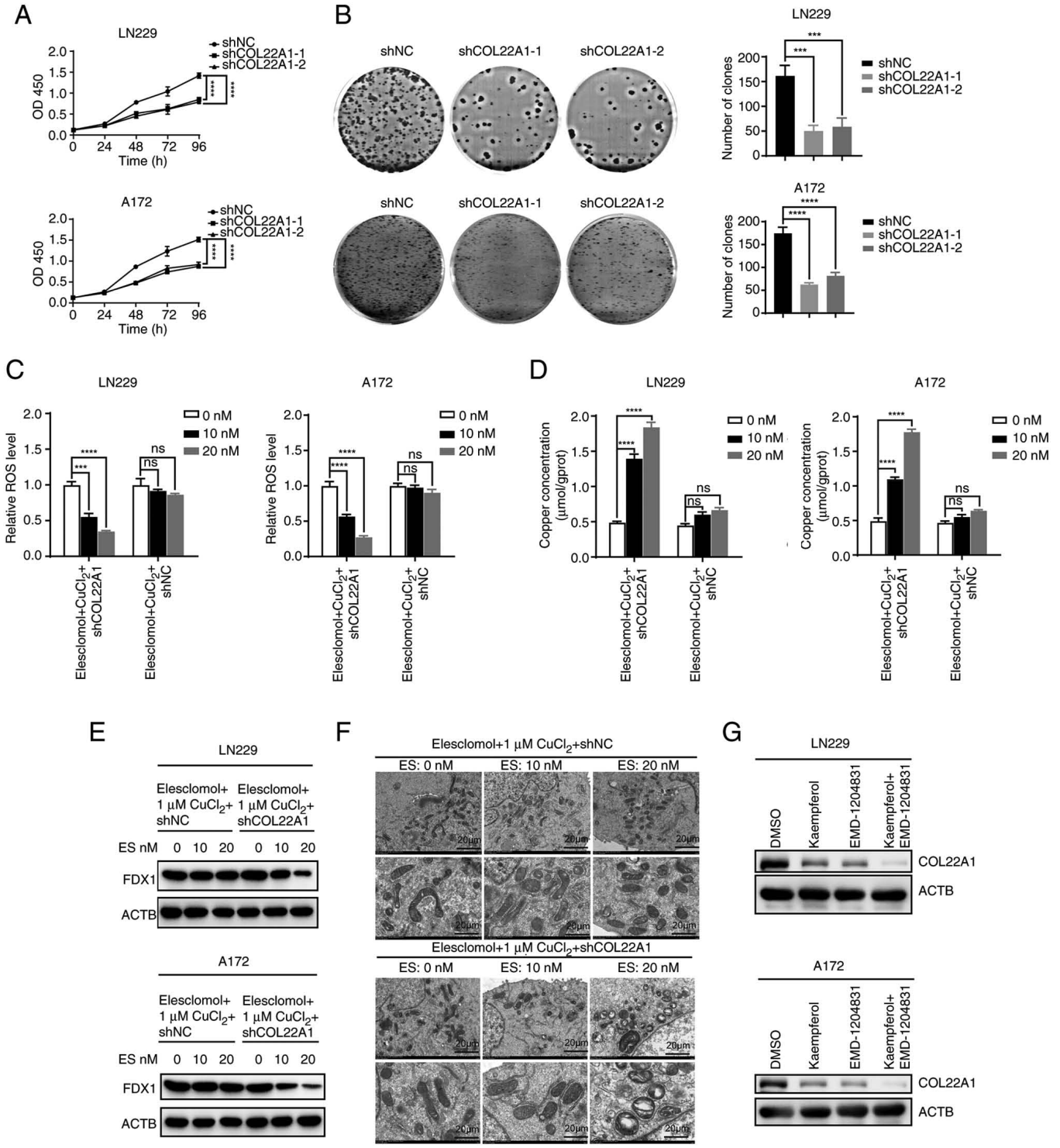

Figure 7. Silencing of COL22A1 enhances glioblastoma cuproptosis. (A) Cell Counting Kit-8 assays were performed in shNC and shCOL22A1 LN229 and A172 cell lines. (B) Colony formation assays were performed in shNC and shCOL22A1 LN229 and A172 cell lines. (C) ROS levels of shNC and shCOL22A1 LN229 and A172 cells exposed to increasing doses of elesclomol for 24 h. (D) Concentration of copper following exposure to increasing doses of elesclomol for 24 h in shNC and shCOL22A1 LN229 and A172 cell lines. (E) Western blotting detecting the representative marker (FDX1) of cuproptosis in shNC or shCOL22A1 LN229 and A172 cells following exposure to increasing doses of elesclomol for 24 h. (F) Transmission electron microscopy images were captured following exposure to increasing doses of elesclomol for 24 h in shNC or shCOL22A1 LN229 cells. Scale bar, 20 μm. (G) Protein levels of COL22A1 in LN229 and A172 cells treated with DMSO or kaempferol combined with EMD-1204831 examined by western blotting. Data are presented as the mean ± SD of three experiments. ***P<0.001, ****P<0.0001 vs. controls. ACTB, actin β; COL22A1, collagen type XXII α1 chain; ES, elesclomol; FDX1, ferredoxin 1; NC, negative control; ns, not significant; OD, optical density; ROS, reactive oxygen species; sh, short hairpin RNA.

copper ion-induced cell death has not been elucidated (25). Cuproptosis can induce tumor cell death, including GBM cell death; however, the underlying mechanisms remain largely unknown and warrant investigation (4). Exploring the molecular mechanisms by which copper toxicity leads to cell death is expected to provide a deeper understanding

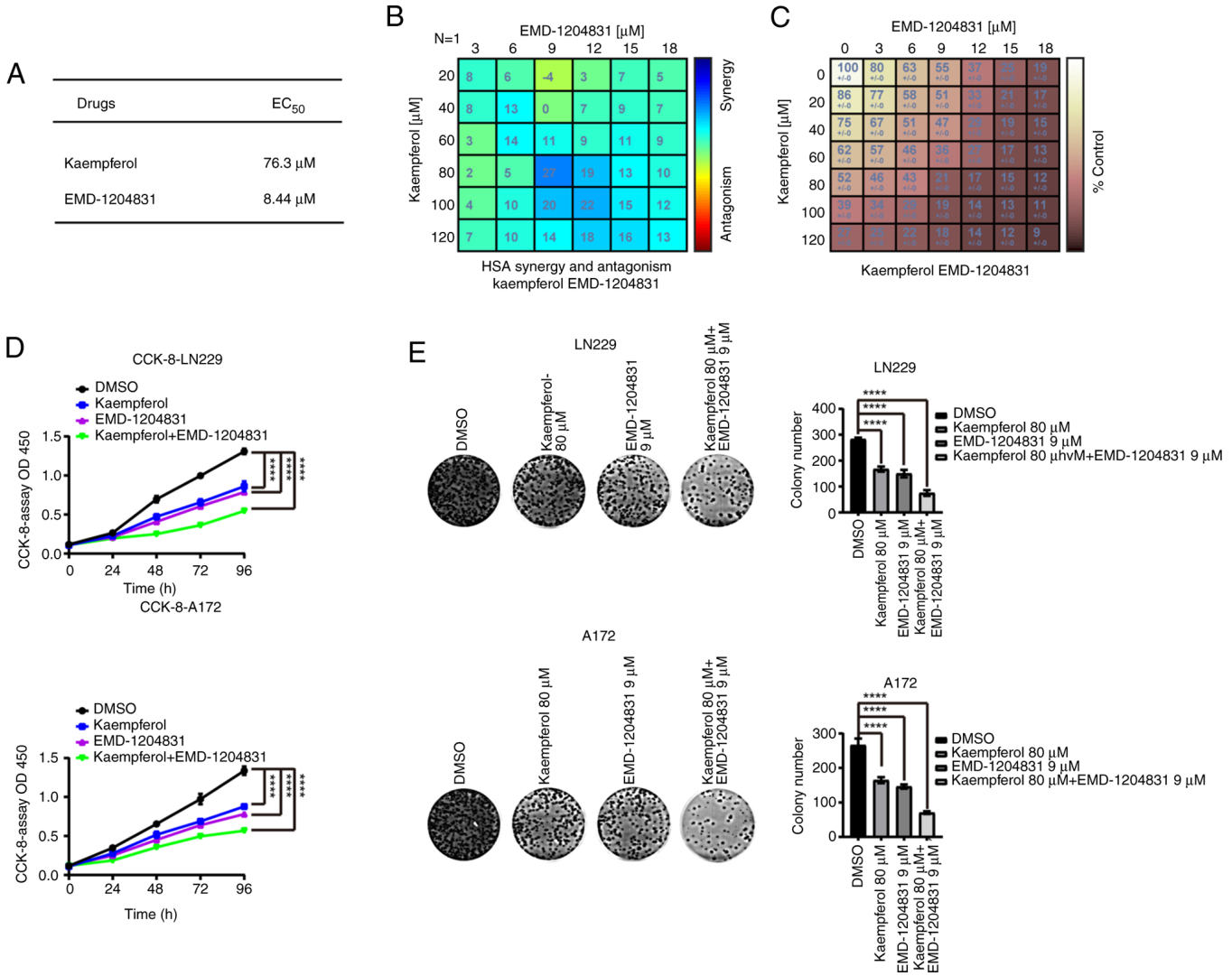

Figure 8. EMD-1204831 and kaempferol synergistically treat glioblastoma *in vitro*. (A) EC_{50} of kaempferol and EMD-1204831. (B) Proper concentrations were detected in LN229 cell lines that were treated with EMD-1204831 in combination with kaempferol. (C) Cell percentages were detected in LN229 cell lines that were treated with EMD-1204831 in combination with kaempferol. (D) CCK-8 assay of LN229 and A172 cells that were treated with EMD-1204831 in combination with kaempferol. (E) Colony formation assays were performed in LN229 and A172 cell lines that were treated with EMD-1204831 in combination with kaempferol. Data are presented as the mean ± SD of three experiments. ****P<0.0001 vs. controls. CCK-8, Cell Counting Kit-8; EC_{50}, median effect concentration; HSA, highest single agent; OD, optical density.

of copper imbalance in human diseases and the development of treatment strategies. Using LASSO regression analysis, a prediction model of genes linked to cuproptosis in GBM was created. In parallel, the relationship between the GBM risk score and methylation, DNA mutation or scRNA-seq data was investigated. The results of the multiomics analysis showed that the prognostic pattern was associated with the immune microenvironment, and kaempferol and EMD-1204831 had a collaborative inhibitory effect on GBM cells. The present findings provide a novel predictive model for the diagnosis of GBM based on cuproptosis-related genes, and novel targets and potential therapeutic options for its treatment.

Cluster analysis was adopted according to the expression levels of cuproptosis genes in GBM to obtain different cuproptosis expression level groups. Subsequently, DEG analysis and Cox proportional hazards model analysis between the two groups of patients were performed, the acquired genes were examined by LASSO regression, and the risk score genes were used to establish a prognostic model related to cuproptosis in GBM. A total of nine genes, including *AEBP1*, *NSUN5*, *MED10*, *CCM2*, *OSMR*, *RPL39L*, *EN2*, *COL22A1* and *DNAJC30*, were related to GBM. The fibril-associated collagens with interrupted triple-helices protein family is represented structurally by the collagen encoded by the COL22A1 gene on human chromosome 8q24.2. The extracellular matrix protein known as collagen XXII, a unique gene product, is exclusively found at tissue junctions in the skin, muscle, articular cartilage, heart and tendon. At the tendon junction, collagen XXII is deposited in the basement membrane region (26). Transcriptional regulation of COL22A1 suppresses nasopharyngeal carcinoma cell senescence through G_1/S arrest (27). High proliferation and recurrence rates of squamous cell carcinoma of the head and neck are positively associated with high COL22A1 expression, which can be used as a prognostic indicator for this tumor, and COL22A1 is also closely related to the prognosis

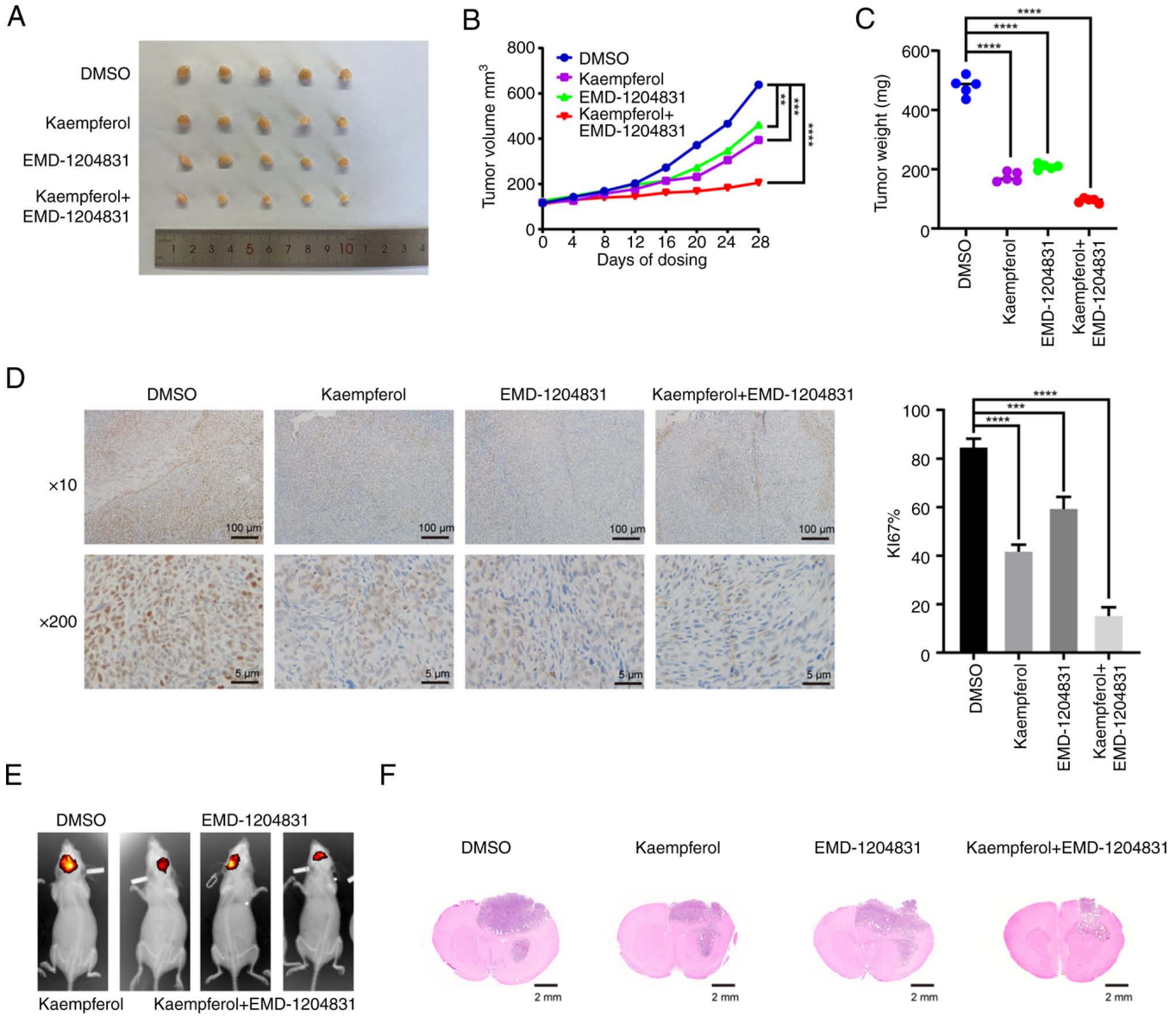

Figure 9. EMD-1204831 and kaempferol synergistically treat glioblastoma *in vivo*. (A) Gross tumor tissue images of each group. (B) Statistical analysis of tumor tissue volume in each group. (C) Statistical analysis of tumor tissue weight in each group. (D) Ki67 staining of tumor tissue in each group. Scale bar, 5 or 100 μm as indicated. Magnification, x10 or x200 as indicated. (E) Intracranial tumorigenesis mice were treated with kaempferol, EMD-1204831 or the combination. Representative tumor images. (F) H&E staining of tumors. Scale bar, 2 mm. Data are presented as the mean ± SD of three experiments. *P<0.01, ***P<0.001, ****P<0.0001 vs. controls.

of osteosarcoma (28,29). A pooled analysis or Kaplan-Meier survival analysis was performed for these nine genes in the training and validation sets to calculate AUC values and it was verified that the risk scores of the predictive models were consistent with the condition of patients, which means this prognostic model could predict the survival status of patients. Overall, different approaches were taken in both the training set and validation set to check the usefulness and reliability of the model.

scRNA-seq technology refers to high-throughput sequencing of genetic information such as the genome, transcriptome and epigenome at the single-cell level. scRNA-seq reflects the heterogeneity and genetic information of rare cells that cannot be obtained by sequencing mixed samples. It reveals the gene structure and gene expression status of individual cells and provides more detailed information on individual cells (30). The status of immune cell heterogeneity was investigated by scRNA-seq (31). The application and development of scRNA-seq technology is a novel method to develop treatments for neurodegenerative diseases and identify targets and biomarkers (32). GBM samples were sorted into malignant, normal and no classification groups based on scRNA-seq data. Among the three groups, the highest risk score was observed in the malignant group, whereby the risk score could assess tumor development and progression. Next, a timeline analysis of risk scores and associated genes was performed, which showed that risk scores and associated genes gradually increased with tumor progression. The aforementioned results demonstrated that the present prognostic model could predict tumor occurrence to some extent.

Chemosensitivity analysis revealed a strong association between risk score-related genes and the drug susceptibility

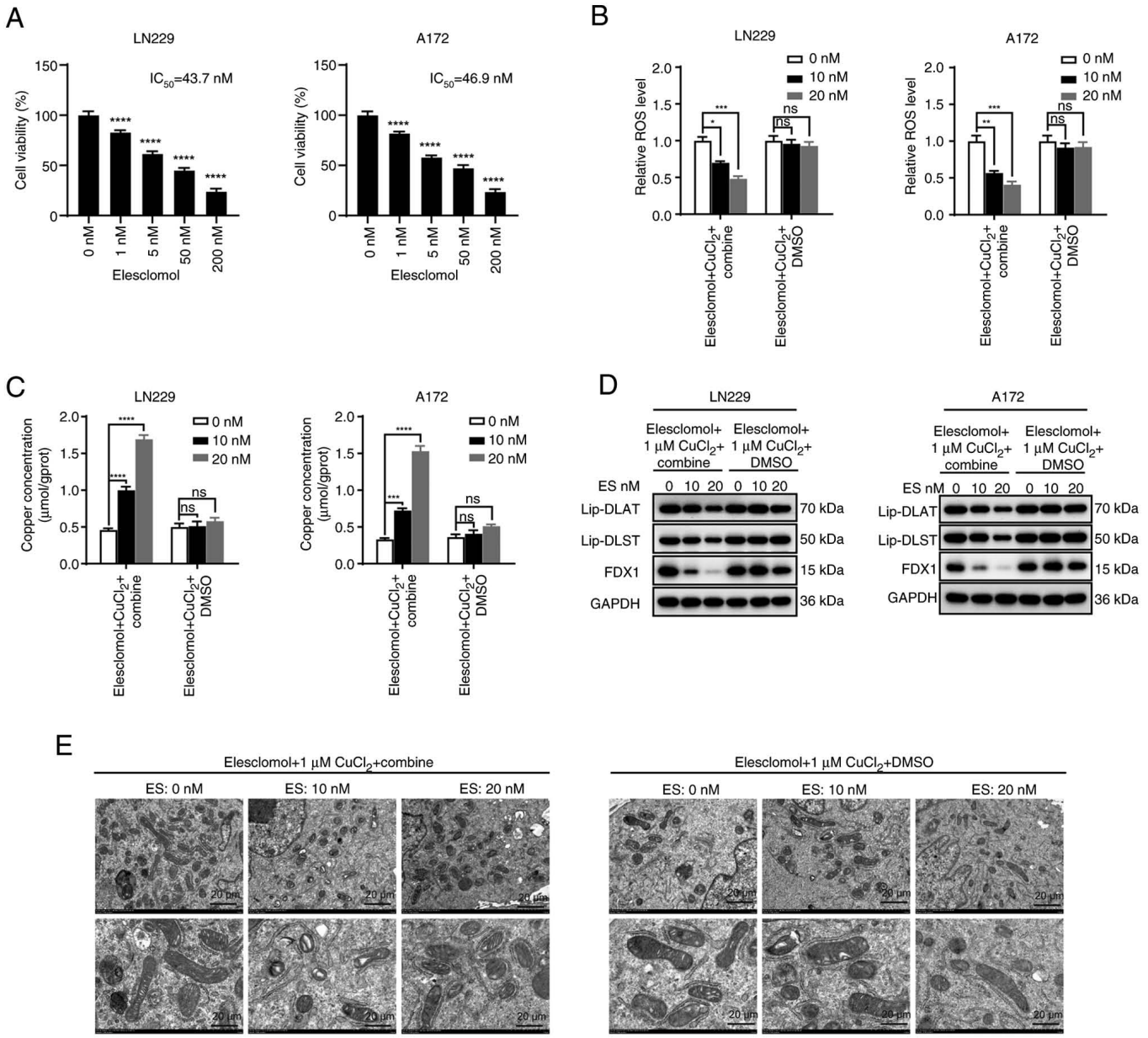

Figure 10. Combination of EMD-1204831 and kaempferol sensitizes glioblastoma to cuproptosis inducers. (A) Cell viability of LN229 and A172 cells following exposure to increasing doses of elesclomol for 24 h. (B) ROS level of LN229 and A172 cells treated with DMSO or kaempferol combined with EMD-1204831 while exposed to increasing doses of elesclomol for 24 h. (C) Concentration of copper following exposure to increasing doses of elesclomol for 24 h in LN229 and A172 cells treated with DMSO or kaempferol combined with EMD-1204831. (D) Representative markers of cuproptosis in LN229 and A172 cells treated with DMSO or kaempferol combined with EMD-1204831 while exposed to increasing doses of elesclomol for 24 h examined by western blotting. (E) Transmission electron microscopy images captured following exposure to increasing doses of elesclomol for 24 h in LN229 cells treated with DMSO or kaempferol combined with EMD-1204831. Scale bar, 20 μm. Data are presented as the mean ± SD of three experiments. *P<0.05, **P<0.01, ***P<0.001, ****P<0.0001 vs. control. DLAT, dihydrolipoamide S-acetyltransferase; DLST, dihydrolipoamide S-succinyltransferase; ES, elesclomol; FDX1, ferredoxin 1; Lip, lipoylation; ns, not significant; ROS, reactive oxygen species.

of several widely used chemotherapeutic medications. The present study also revealed that the risk score exhibited an obvious correlation with EMD-1204831 indicating that this drug may be useful in treating GBM based on the prognostic model. Furthermore, the present experiments also verified this association. EMD-1204831 treatment is associated with potent tumor growth suppression and regression; however, to the best of our knowledge, the specific mechanism of action is unknown (15,33). The present study attempted to investigate combination therapy based on integrative traditional Chinese and Western medicine. Therefore, drug sensitivity, network pharmacology and molecular docking analyses were performed, and only COL22A1 could be targeted by EMD-1204831 and kaempferol simultaneously, according to the overlap between the prognostic genes and the genes targeted by Ginseng. Although COL22A1 was not the most markedly altered protein compared with in normal tissues based on immunohistochemistry data, it was selected for further study. Kaempferol was found to target the COL22A1 protein in prognostic models based on molecular docking and network pharmacology analyses. Kaempferol is a natural compound and the most common flavonoid found

widely in vegetables and fruits (34,35). Kaempferol and its glycosylated derivatives have been shown to have numerous functions, including antioxidant, anti-inflammatory, antimicrobial, anticancer, cardioprotective, neuroprotective, antidiabetic, anti-osteoporotic, estrogenic/antiestrogenic, anxiolytic, analgesic and antiallergic activities (36). Several anticancer effects of kaempferol have been reported, including in breast cancer, gastric cancer, prostate cancer, bladder cancer, cervical cancer, colon cancer, liver cancer, lung cancer, ovarian cancer and leukemia (37-39). Kaempferol can also inhibit the invasion/migration of GBM cells by inhibiting 12-O-tetradecanoylphorbol-13-acetate-induced protein kinase Cα/ERK/NF-κB activation, migration and MMP-9 activation (40). Since the studies of kaempferol and EMD-1204831 in GBM are not precise enough, a comprehensive mechanistic analysis of their anti-GBM action was conducted. The two drugs synergistically inhibited the proliferation of GBM cells. Through cluster analysis and LASSO regression analysis, the prognostic cuproptosis-related genes in GBM were identified. Furthermore, the drugs EMD-1214063 and kaempferol could target one of the aforementioned genes, COL22A1, simultaneously based on the drug sensitivity analysis and network pharmacology. Therefore, we hypothesized that these two drugs exert their function through the same target and validated their synergistic effect in subsequent experiments. EMD-1204831 is a c-Met inhibitor that has been reported to inhibit cancer cell proliferation (14); however, to the best of our knowledge, its mechanism of action has not been studied. As one of the natural flavonoids, kaempferol is often considered to inhibit tumors (36,41). However, to the best of our knowledge, the application of kaempferol in GBM has not yet been reported. Kaempferol, the main ingredient in natural medicine, has no clearly-defined purpose (36,37). In summary, the present study has found a reliable method for the potential treatment of GBM and a theoretical basis for the treatment of GBM based on integrated traditional Chinese and Western medicine.

In conclusion, the purpose of the present study was to investigate the important role of cuproptosis in the diagnosis and treatment of GBM. First, a cuproptosis-related prediction model was constructed using bioinformatics analysis. The results of single-cell sequencing analysis showed that the risk score calculated by the prognostic model was higher in malignant GBM cell clusters and increased with the progression of malignant tumors. The multiomics analysis revealed that the prognostic pattern was strongly associated with immune system infiltration, DNA methylation and mutations. The combination of kaempferol and EMD-1204831 exhibited improved treatment efficiency in inhibiting GBM progression.

Acknowledgements

Not applicable.

Funding

The present study was supported by the Key Research and Development Project of Liaoning Province (grant no. 2018225040), the Science and Technology Planning Project of Shenyang (grant no. 22-321-33-50), the Special Fund for Clinical Research of Wu Jieping Medical Foundation (grant no. 320.6750.2023-17-13) and the Natural Science Foundation of Liaoning Province (grant no. 2023-BS-046).

Availability of data and materials

The data generated in the present study may be requested from the corresponding author.

Authors' contributions

YC was involved in conceptualization, performed experiments and wrote the original draft. HX and HP confirm the authenticity of all the raw data. YZ was involved in conceptualization and funding acquisition. HY, QL, RS, JS, HL and JL performed experiments. HX performed experiments, revised and edited the manuscript, and acquired funding. HP performed experiments, acquired funding and supervised the study. All authors have read and approved the final manuscript.

Ethics approval and consent to participate

The present study was carried out in strict accordance with the recommendations in the Guide for the Care and Use of Laboratory Animals of the National Institutes of Health. All procedures that involved animals were approved by the Experimental Animal Ethics Committee: China Medical University (approval no. CMUXN2023010; approval date, March 9, 2023; Shenyang, China). All surgery was performed under isoflurane anesthesia, and all efforts were made to minimize suffering.

Patient consent for publication

Not applicable.

Competing interests

The authors declare that they have no competing interests.

References

1. Ostrom QT, Gittleman H, Liao P, Rouse C, Chen Y, Dowling J, Wolinsky Y, Kruchko C and Barnholtz-Sloan J: CBTRUS statistical report: Primary brain and central nervous system tumors diagnosed in the United States in 2007-2011. Neuro Oncol 16 (Suppl 4): iv1-iv63, 2014.
2. Salcman M: Glioblastoma multiforme. Am J Med Sci 279: 84-94, 1980.
3. Dolecek TA, Propp JM, Stroup NE and Kruchko C: CBTRUS statistical report: Primary brain and central nervous system tumors diagnosed in the United States in 2005-2009. Neuro Oncol 14 (Suppl 5): v1-v49, 2012.
4. Ala A, Walker AP, Ashkan K, Dooley JS and Schilsky ML: Wilson's disease. Lancet 369: 397-408, 2007.
5. Kahlson MA and Dixon SJ: Copper-induced cell death. Science 375: 1231-1232, 2022.
6. Grasso M, Bond GJ, Kim YJ, Boyd S, Matson Dzebo M, Valenzuela S, Tsang T, Schibrowsky NA, Alwan KB, Blackburn NJ, *et al*: The copper chaperone CCS facilitates copper binding to MEK1/2 to promote kinase activation. J Biol Chem 297: 101314, 2021.

7. Jia W, Tian H, Jiang J, Zhou L, Li L, Luo M, Ding N, Nice EC, Huang C and Zhang H: Brain-targeted HFn-Cu-REGO nanoplatform for site-specific delivery and manipulation of autophagy and cuproptosis in glioblastoma. Small 19: e2205354, 2023.
8. Tsvetkov P, Detappe A, Cai K, Keys HR, Brune Z, Ying W, Thiru P, Reidy M, Kugener G, Rossen J, *et al*: Mitochondrial metabolism promotes adaptation to proteotoxic stress. Nat Chem Biol 15: 681-689, 2019.
9. Yang L, Zhang Y, Wang Y, Jiang P, Liu F and Feng N: Ferredoxin 1 is a cuproptosis-key gene responsible for tumor immunity and drug sensitivity: A pan-cancer analysis. Front Pharmacol 13: 938134, 2022.
10. Brem S, Grossman SA, Carson KA, New P, Phuphanich S, Alavi JB, Mikkelsen T and Fisher JD; New Approaches to Brain Tumor Therapy CNS Consortium: Phase 2 trial of copper depletion and penicillamine as antiangiogenesis therapy of glioblastoma. Neuro Oncol 7: 246-253, 2005.
11. Li Y, Hu J, Guan F, Song L, Fan R, Zhu H, Hu X, Shen E and Yang B: Copper induces cellular senescence in human glioblastoma multiforme cells through downregulation of Bmi-1. Oncol Rep 29: 1805-1810, 2013.
12. Lun X, Wells JC, Grinshtein N, King JC, Hao X, Dang NH, Wang X, Aman A, Uehling D, Datti A, *et al*: Disulfiram when combined with copper enhances the therapeutic effects of temozolomide for the treatment of glioblastoma. Clin Cancer Res 22: 3860-3875, 2016.
13. Li X, Ma Z and Mei L: Cuproptosis-related gene SLC31A1 is a potential predictor for diagnosis, prognosis and therapeutic response of breast cancer. Am J Cancer Res 12: 3561-3580, 2022.
14. Zhang Z, Zeng X, Wu Y, Liu Y, Zhang X and Song Z: Cuproptosis-related risk score predicts prognosis and characterizes the tumor microenvironment in hepatocellular carcinoma. Front Immunol 13: 925618, 2022.
15. Bladt F, Faden B, Friese-Hamim M, Knuehl C, Wilm C, Fittschen C, Grädler U, Meyring M, Dorsch D, Jaehrling F, *et al*: EMD 1214063 and EMD 1204831 constitute a new class of potent and highly selective c-Met inhibitors. Clin Cancer Res 19: 2941-2951, 2013.
16. Jessa S, Mohammadnia A, Harutyunyan AS, Hulswit M, Varadharajan S, Lakkis H, Kabir N, Bashardanesh Z, Hébert S, Faury D, *et al*: K27M in canonical and noncanonical H3 variants occurs in distinct oligodendroglial cell lineages in brain midline gliomas. Nat Genet 54: 1865-1880, 2022.
17. Arnone AA, Tsai YT, Cline JM, Wilson AS, Westwood B, Seger ME, Chiba A, Howard-McNatt M, Levine EA, Thomas A, *et al*: Endocrine-targeting therapies shift the breast microbiome to reduce estrogen receptor-α breast cancer risk. Cell Rep Med 6: 101880, 2025.
18. Wu Z, Li W, Zhu H, Li X, Zhou Y, Chen Q, Huang H, Zhang W, Jiang X and Ren C: Identification of cuproptosis-related subtypes and the development of a prognostic model in glioma. Front Genet 14: 1124439, 2023.
19. Nishiyama A and Nakanishi M: Navigating the DNA methylation landscape of cancer. Trends Genet 37: 1012-1027, 2021.
20. Jiang H and Bu L: Progress in the treatment of lung adenocarcinoma by integrated traditional Chinese and Western medicine. Front Med (Lausanne) 10: 1323344, 2024.
21. Chen L, Xu YX, Wang YS, Ren YY, Chen YM, Zheng C, Xie T, Jia YJ and Zhou JL: Integrative Chinese-Western medicine strategy to overcome docetaxel resistance in prostate cancer. J Ethnopharmacol 331: 118265, 2024.
22. Lin J, Sun L, Chen H, Chen W, Zhang Z, Cao Y and Lin L: Chinese and Western integrative medicine for stage IIIb-IVb non-small cell lung cancer: Design and rationale of a multi-center, prospective registry (NSCLC-Chinese and Western integrative medicine cohort). Integr Cancer Ther 22: 15347354231185109, 2023.
23. Komori T: The 2016 WHO classification of tumours of the central nervous system: The major points of revision. Neurol Med Chir (Tokyo) 57: 301-311, 2017.
24. Wu W, Klockow JL, Zhang M, Lafortune F, Chang E, Jin L, Wu Y and Daldrup-Link HE: Glioblastoma multiforme (GBM): An overview of current therapies and mechanisms of resistance. Pharmacol Res 171: 105780, 2021.
25. Chen L, Min J and Wang F: Copper homeostasis and cuproptosis in health and disease. Signal Transduct Target Ther 7: 378, 2022.
26. Koch M, Schulze J, Hansen U, Ashwodt T, Keene DR, Brunken WJ, Burgeson RE, Bruckner P and Bruckner-Tuderman L: A novel marker of tissue junctions, collagen XXII. J Biol Chem 279: 22514-22521, 2004.
27. Huang ML and Luo WL: Engrailed homeobox 1 transcriptional regulation of COL22A1 inhibits nasopharyngeal carcinoma cell senescence through the G1/S phase arrest. J Cell Mol Med 26: 5473-5485, 2022.
28. Misawa K, Kanazawa T, Imai A, Endo S, Mochizuki D, Fukushima H, Misawa Y and Mineta H: Prognostic value of type XXII and XXIV collagen mRNA expression in head and neck cancer patients. Mol Clin Oncol 2: 285-291, 2014.
29. Pan R, Pan F, Zeng Z, Lei S, Yang Y, Yang Y, Hu C, Chen H and Tian X: A novel immune cell signature for predicting osteosarcoma prognosis and guiding therapy. Front Immunol 13: 1017120, 2022.
30. Lei Y, Tang R, Xu J, Wang W, Zhang B, Liu J, Yu X and Shi S: Applications of single-cell sequencing in cancer research: Progress and perspectives. J Hematol Oncol 14: 91, 2021.
31. Papalexi E and Satija R: Single-cell RNA sequencing to explore immune cell heterogeneity. Nat Rev Immunol 18: 35-45, 2018.
32. Ofengeim D, Giagtzoglou N, Huh D, Zou C and Yuan J: Single-Cell RNA sequencing: Unraveling the brain one cell at a time. Trends Mol Med 23: 563-576, 2017.
33. Walker K and Padhiar M: AACR-NCI-EORTC--21st international symposium. Molecular targets and cancer therapeutics-Part 2. IDrugs 13: 10-12, 2010.
34. Devi KP, Malar DS, Nabavi SF, Sureda A, Xiao J, Nabavi SM and Daglia M: Kaempferol and inflammation: From chemistry to medicine. Pharmacol Res 99: 1-10, 2015.
35. Yang RY, Lin S and Kuo G: Content and distribution of flavonoids among 91 edible plant species. Asia Pac J Clin Nutr 17 (Suppl 1): S275-S279, 2008.
36. Calderón-Montaño JM, Burgos-Morón E, Pérez-Guerrero C and López-Lázaro M: A review on the dietary flavonoid kaempferol. Mini Rev Med Chem 11: 298-344, 2011.
37. Kim TW, Lee SY, Kim M, Cheon C and Ko SG: Kaempferol induces autophagic cell death via IRE1-JNK-CHOP pathway and inhibition of G9a in gastric cancer cells. Cell Death Dis 9: 875, 2018.
38. Wang X, Yang Y, An Y and Fang G: The mechanism of anticancer action and potential clinical use of kaempferol in the treatment of breast cancer. Biomed Pharmacother 117: 109086, 2019.
39. Tie F, Ding J, Hu N, Dong Q, Chen Z and Wang H: Kaempferol and kaempferide attenuate oleic acid-induced lipid accumulation and oxidative stress in HepG2 cells. Int J Mol Sci 22: 8847, 2021.
40. Lin CW, Shen SC, Chien CC, Yang LY, Shia LT and Chen YC: 12-O-tetradecanoylphorbol-13-acetate-induced invasion/migration of glioblastoma cells through activating PKCalpha/ERK/NF-kappaB-dependent MMP-9 expression. J Cell Physiol 225: 472-481, 2010.
41. Imran M, Salehi B, Sharifi-Rad J, Aslam Gondal T, Saeed F, Imran A, Shahbaz M, Tsouh Fokou PV, Umair Arshad M, Khan H, *et al*: Kaempferol: A key emphasis to its anticancer potential. Molecules 24: 2277, 2019.